

Computational Approaches to Many-Body Dynamics of Unstable Nuclear Systems

Alexander Volya

Department of Physics, Florida State University, Tallahassee, FL 32306-4350, USA

Abstract

The goal of this presentation is to highlight various computational techniques used to study dynamics of quantum many-body systems. We examine the projection and variable phase methods being applied to multi-channel problems of scattering and tunneling; here the virtual, energy-forbidden channels and their treatment are of particular importance. The direct time-dependent solutions using Trotter–Suzuki propagator expansion provide yet another approach to exploring the complex dynamics of unstable systems. While presenting computational tools, we briefly revisit the general theory of the quantum decay of unstable states. The list of questions here includes those of the internal dynamics in decaying systems, formation and evolution of the radiating state, and low-energy background that dominates at remote times. Mathematical formulations and numerical approaches to time-dependent problems are discussed using the quasi-stationary methods involving effective non-Hermitian Hamiltonian formulation.

Keywords: *Quantum many-body dynamics, Time-Dependent Continuum Shell Model; Variable Phase Method; Trotter–Suzuki propagator expansion*

1 Introduction

There is no physical system that is truly isolated from the rest of the world, the closed system idealization may be convenient but becomes poor or completely invalid for many questions of modern-day science. In nuclear physics, as interests shift towards weakly bound, unbound or even dynamically evolving reaction states, the theoretical approaches for dealing with unstable dynamics of open quantum systems with multiple degrees of freedom should be revisited. The availability of advanced computational technologies calls forth innovative thinking and new philosophies in addressing these types of quantum many-body problems. In this presentation, using different models and realistic examples from the world of nuclear physics, we discuss computational strategies and techniques for dealing with dynamically unstable many-body systems. The *Nuclear Theory in the Supercomputing Era* venue is especially timely and allows us to put emphasis on some of the techniques, that due to their computational nature, remained behind the curtains in a number of recent investigations [1–3].

2 Intrinsic degrees of freedom in reactions

2.1 Projection method

Let us start by illustrating the difficulties that one faces while trying to reformulate reaction problems using the basis projection methods typical for structure physics;

Proceedings of the International Conference ‘Nuclear Theory in the Supercomputing Era — 2014’ (NTSE-2014), Khabarovsk, Russia, June 23–27, 2014. Eds. A. M. Shirokov and A. I. Mazur. Pacific National University, Khabarovsk, Russia, 2016, p. 35.

<http://www.ntse-2014.khb.ru/Proc/Volya.pdf>.

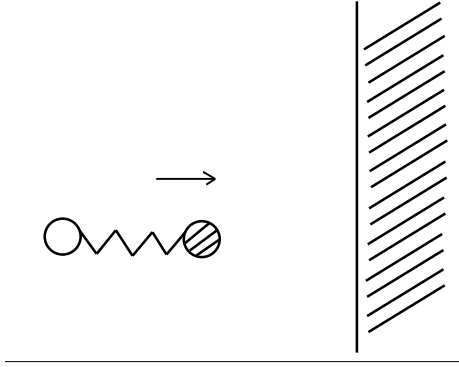


Figure 1: Schematic picture of scattering. A composite system of two particles bound by a harmonic oscillator potential scatters off an infinite wall. One of the particles does not interact with the wall, at the same time the wall is impenetrable for the second particle.

see also Refs. [2, 4]. Consider a model of scattering illustrated in Fig. 1. In this one-dimensional problem two particles with masses μ_1 and μ_2 comprise a composite system of unit mass $\mu_1 + \mu_2 = 1$. The system can be described with the center-of-mass and relative coordinates, $X = \mu_1 x_1 + \mu_2 x_2$ and $x = x_1 - x_2$, respectively. The two particles are confined by a potential $v(x)$. The intrinsic Hamiltonian

$$h = -\frac{1}{\mu} \frac{\partial^2}{\partial x^2} + v(x) \quad (1)$$

is assumed to have a complete set of discrete eigenstates $\psi_n(x)$ with corresponding intrinsic energies ϵ_n :

$$h\psi_n(x) = \epsilon_n\psi_n(x), \quad n = 0, 1, 2, \dots$$

Here the reduced mass is $\mu = \mu_1\mu_2$ and we select our units so that $\hbar^2/2 = 1$. We assume that this system scatters off an infinite wall and the wall interacts only with the second particle. Therefore the full Hamiltonian is

$$H = -\frac{\partial^2}{\partial X^2} + U(x_2) + h, \quad \text{where} \quad U(x_2) = \begin{cases} \infty & \text{if } x_2 \geq 0 \\ 0 & \text{if } x_2 < 0 \end{cases}. \quad (2)$$

As illustrated in Fig. 1, we assume that the incident beam is traveling from the left and contains the projectiles in an intrinsic state (channel) n . A complete set of reflected waves is characterized by the amplitudes R_{nm} defined here so that $|R_{mn}|^2$ represents the probability for the initial beam in channel n to reflect in channel m ; $R_{nm} = R_{mn}$ due to time-reversal invariance. The scattering wave function is

$$\Phi(X, x) = \frac{e^{iK_n X}}{\sqrt{|K_n|}} \psi_n(x) + \sum_{m=0}^{\infty} \frac{R_{mn}}{\sqrt{|K_m|}} e^{-iK_m X} \psi_m(x), \quad (3)$$

where

$$K_n(E) = \sqrt{(E - \epsilon_n)} \quad (4)$$

is the center-of-mass momentum of the two-particle system while in the n^{th} intrinsic state, and E is the total energy.

A channel n is considered to be open if $E \geq \epsilon_n$ and the corresponding momentum K_n is real. The conservation of particle-number in all open channels necessitates $\sum_{m \in \text{open}} |R_{mn}|^2 = 1$. The channel is closed if $E < \epsilon_n$, in which case K_n is purely imaginary. We stress that the principal value of the square root is implied in Eq. (4).

The boundary condition set by an impenetrable wall,

$$\Phi(X, x) = 0 \quad \text{at} \quad x_2 = 0, \quad (5)$$

is to be used for determining the set of coefficients R_{mn} . Since the center-of-mass coordinate $X = \mu_1 x$ at $x_2 = 0$, the boundary condition can be expressed in the intrinsic coordinate x only, $\Phi(\mu_1 x, x) = 0$. Therefore we can project the reaction problem onto a complete set of intrinsic basis states, which leads to the following linear equation

$$\sum_m \frac{D_{n'm}[-i\mu_1(K_n + K_m)]}{\sqrt{|K_m|}} R_{mn} = -\frac{\delta_{n'n}}{\sqrt{|K_n|}}, \quad (6)$$

where the matrix D is defined as

$$D_{mn}(\varkappa) = \langle \psi_m | \exp(\varkappa x) | \psi_n \rangle. \quad (7)$$

Equation (6) represents a typical mathematical challenge associated with the formulation of reaction problems where reaction states are projected onto the intrinsic states; see also Section 3. It is a linear algebra problem where the construction of the scattering matrix amounts to matrix inversion in the projected space. The scattering energy E is a running parameter here, and studies of scattering at different energies is therefore time consuming. And, finally, the underlying matrix is highly singular and there are convergence issues. The latter difficulty is the one that we would like to illustrate using this example.

If the two particles forming a composite system are bound by a harmonic oscillator confinement, $v(x) = \mu\omega^2 x^2/2$ in Eq. (1), the D -matrix is known analytically [2]. Then to solve the problem we truncate the channel space at some large number N of oscillator quanta, and solve Eq. (6) using standard numerical techniques. This turns out to be a difficult task; the matrix element $D_{mn}(\varkappa)$ for virtual channels, where \varkappa is real, are exponentially large, making the process of matrix inversion difficult and numerically unstable [2, 5, 6]. As shown in Fig. 2, left panel, the absolute values of the reflection amplitudes, $R_n \equiv R_{0n}$, exponentially diverge for increasingly remote virtual channels.

While it is possible to overcome the numerical issues, further examination shows that the approach has fundamental flaws. In Fig. 2, right panel, the phase shift, defined as $e^{2i\delta} = -R_{00}$, is shown as a function of N . While satisfactory and seemingly convergent results can be easily found for the cases where the mass of the non-interacting particle is small, in general the results start oscillating as N increases; situations where the non-interacting particle is heavy and therefore deeply penetrates the wall, are particularly difficult to handle. It was emphasized in Refs. [2, 4] that there is no numerical convergence with increasing N .

2.2 Variable Phase Method

The above example shows that reaction problems call for new techniques. One approach, based on the Variable Phase Method (VPM), see Ref. [7], is proposed in Ref. [2]. The VPM is an effective technique for solving the coupled-channel problem of the form

$$\left[\frac{\partial^2}{\partial X^2} + K_n^2 \right] \Psi_n(X) - \sum_{n'} V_{nn'}(X) \Psi_{n'}(X) = 0, \quad (8)$$

where scattering observables are to be expressed relative to free-space solutions normalized to unit current

$$\Xi_{nn'}^{\pm}(X) = \frac{e^{\pm iK_n X}}{\sqrt{-2iK_n}} \delta_{nn'}; \quad (9)$$

the \pm sign corresponds to a wave moving in the right/left direction. In the VPM approach, the coupled-channel Schrödinger equation (8) is reformulated as a set of first order differential equations for dynamic reflection and transmission amplitude

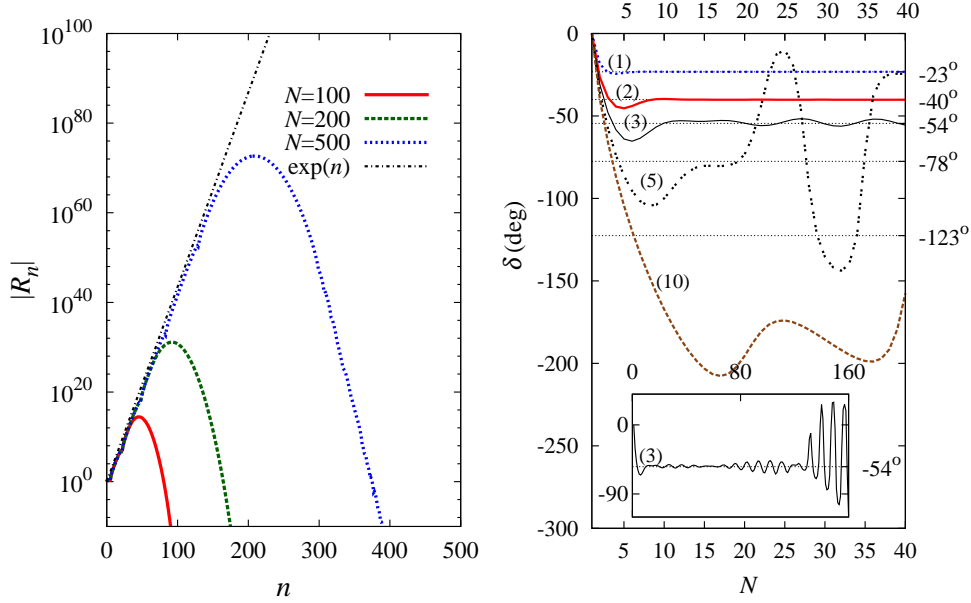


Figure 2: This figure refers to a system of two particles bound by a harmonic oscillator confinement, which collides with an infinite wall. The incident kinetic energy is exactly half of the oscillator quantum so that only the ground state channel is open. Left panel: For a system where $\mu_1 = \mu_2$ the absolute values of amplitudes $|R_n| \equiv |R_{0n}|$ in virtual channels are shown as functions of n assuming different truncations N . The asymptotic dependence is illustrated with the straight line “ $\exp(n)$ ”. Right panel: The phase shift defined for a single open channel as $e^{2i\delta} = -R_{00}$, is plotted as a function of truncation N . The problems with the approach are highlighted by an unstable and oscillatory behavior of the phase shifts. The problem is particularly severe when the non-interacting particle of mass μ_1 is heavy. Different curves show phase-shifts for different mass ratios $\mu_1/\mu_2 = 1, 2, 3, 5, 10$, as labeled; the exact values obtained with Variable Phase Method (see Section 2.2) are shown by the horizontal grid lines with the tic-marks on the right. Inset shows the case when $\mu_1/\mu_2 = 3$ extending the study to considerably large values of N and emphasizing that for any choice of parameters the approach fails at some point.

matrices $R_{nn'}(X')$ and $T_{nn'}(X')$. These amplitudes correspond to a potential that is cut at X' , namely, to $V_{nn'}(X)\theta(X - X')$:

$$\frac{dR(X)}{dX} = [(\Xi^+ + R(X)\Xi^-)]V[\Xi^+ + \Xi^-R(X)], \quad R_{nn'}(\infty) = 0, \quad (10)$$

$$\frac{dT(X)}{dX} = T(X)\Xi^-V[\Xi^+ + \Xi^-R(X)], \quad T_{nn'}(\infty) = \delta_{nn'}. \quad (11)$$

These equations being solved from $X = +\infty$ towards $X \rightarrow -\infty$, recover the reflection and transmission amplitudes $R_{nn'}(-\infty) = R_{nn'}$ and $T_{nn'}(-\infty) = T_{nn'}$.

Using factorization of the form

$$\Phi(X, x) = \sum_n \Psi_n(X) \psi_n(x),$$

the Schrödinger equation for the scattering problem described in Fig. 1 can be transformed into a coupled-channel equation (8) for the center-of-mass wave functions $\Psi_n(X)$, where the folded potentials are

$$V_{nn'}(X) = \int_{-\infty}^{\infty} \psi_n^*(x)U(X, x)\psi_{n'}(x)dx. \quad (12)$$

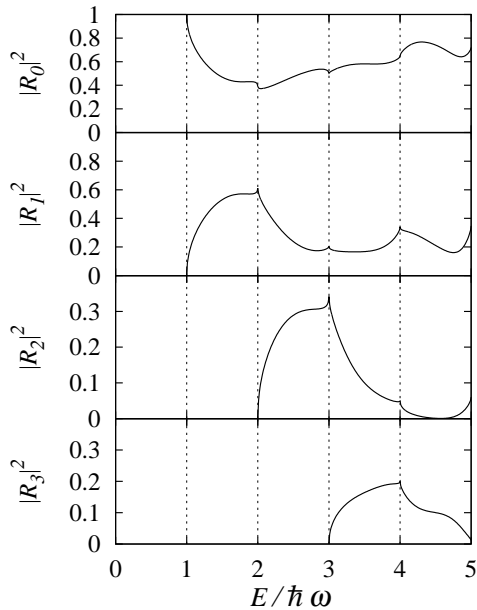


Figure 3: Reflection probabilities in different channels as functions of incident kinetic energy. The incident beam contains a composite projectile in the ground state. Equal masses $\mu_1 = \mu_2$ are assumed for both interacting and non-interacting particles.

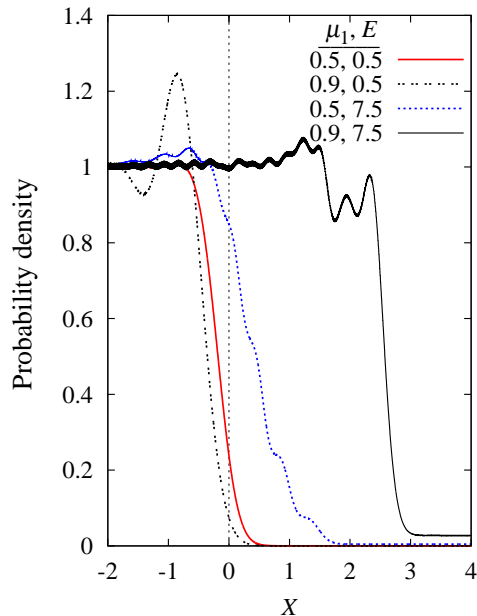


Figure 4: The density of probability for the center of mass of the projectile to be at a location X when it is reflected from an infinite wall at $X = 0$.

Some representative results for the scattering problem where an oscillator-bound system interacts with an infinite wall, are shown in Figs. 3 and 4. The reflection probabilities for different channels are shown in Fig. 3 as functions of incident kinetic energy. The kinetic energy is expressed in units of oscillator $\hbar\omega$, and therefore for each integer value thereof a new channel opens. One can notice typical cusps at thresholds associated with the loss of flux into newly opened channels. In Fig. 4, the probability distribution for the center of mass is shown. The four curves show four of the most representative situations: low and high incident kinetic energies $E = 0.5\hbar\omega$ and $E = 7.5\hbar\omega$, respectively, and two different mass-ratios $\mu_1 = 0.5$ and 0.9 .

2.3 Time-dependent approach

Turning to a time-dependent approach is a natural strategy for dealing with non-stationary systems. There are various computational techniques; see Ref. [8] for some recent tests and comparisons of methods being applied to one-dimensional Schrödinger equation. In time-dependent techniques, a preservation of unitarity is often at the core of computational difficulties: the lack of unitarity could lead to an exponential amplification of numerical noise even for a single channel, while in multi-channel problems, discontinuities near thresholds are particularly challenging. Here we propose and demonstrate another approach that is computationally efficient, even in multi-variable cases, and preserves the unitarity exactly.

The time propagation,

$$\Phi(\mathbf{x}, t) = \exp\left(-\frac{i}{\hbar}Ht\right) \Phi(\mathbf{x}, 0), \quad (13)$$

can be performed by considering separately the potential and kinetic parts

of the Hamiltonian $H = K + V$. In the discretized space of generalized coordinates $\mathbf{x} = \{x_1, x_2, \dots\}$, the potential $V(\mathbf{x})$ is diagonal, so the exponential operator $\exp(-iVt/\hbar)$ can be readily applied. Similarly, in the conjugate momentum space $\mathbf{p} = \{p_1, p_2, \dots\}$, the propagation with kinetic energy operator which is diagonal, is also easy to perform. While the operators K and V do not commute, the time evolution (13) with the combined Hamiltonian can be done efficiently with the Trotter–Suzuki approach [9, 10]. In this approach, the propagation is done in small time steps ΔT ; for each of these steps the evolution operator is approximated as

$$\exp\left(-\frac{i}{\hbar}H\Delta t\right) = \exp\left(-\frac{i}{2\hbar}V\Delta t\right) \exp\left(-\frac{i}{\hbar}K\Delta t\right) \exp\left(-\frac{i}{2\hbar}V\Delta t\right) + O(\Delta t^3). \quad (14)$$

The Fast Fourier Transform allows for an efficient transition between the coordinate and momentum representations so that the exponentials of operators are always applied in the diagonal form. Even with the finite time steps, the unitarity is fully retained; the method is applicable to time-dependent Hamiltonians. The computational cost of two back and forth Fourier transforms involved in each step, is $N \log(N)$ assuming that the coordinate space is discretized into N points. While this appears at first to be higher than the typical $O(N)$ scaling of traditional methods, in practice the cost cN of any high quality method involves a constant factor c that exceeds often $\log(N)$. Moreover, the modern computer hardware often comes with signal processing tools which are optimized at the hardware and software levels to perform the Fast Fourier Transform with an incredible efficiency.

Let us return to the problem of scattering illustrated in Fig. 1. The time dependent picture of the scattering process is shown in Fig. 5 with a series of four plots showing the two-dimensional wave function using a density plot at four different times. The plot of the density projection onto the center-of-mass coordinate X , which is the time-dependent analog of Fig. 4, is shown below each of the four snapshots. The initial wave function at $t = 0$ shown on the first panel, is selected as the ground state wave function for the intrinsic potential, and as a moving Gaussian wave packet for the center of mass coordinate,

$$\Phi(X, x) = \frac{1}{\sqrt{\sigma_0\sqrt{\pi}}} \exp\left[\frac{1}{2\sigma_0^2}(X - X_0)^2 + iK_0X\right] \psi_0(x). \quad (15)$$

In this example, $\sigma_0 = 2$, $X_0 = -5$, and the initial momentum $K_0 = 1$, all quantities are being expressed here in dimensionless units of distance as defined earlier. While this time dependent consideration is different from the stationary state formulation studied above, the series of snapshots for different times shown in Fig. 5 highlights some similar features.

At high energies, the dynamics of virtual excitations is complex; this is illustrated in Fig. 6 where the initial wave packet is selected to have $K_0 = 5$. A semiclassical interpretation can be given to the stages of the process. An initial compression at $t = 1$ is followed by two particles bouncing apart at $t = 2$. Having equal masses, their center of mass remains at the origin but the relative separation x becomes large so that the particles are positioned roughly symmetrically on the opposite sides of the wall. Next, at $t = 3$, the center of mass moves into the $X < 0$ region pressing the interacting particle against the wall. Finally, the system is reflected at $t = 4$ with the initial wave packet being considerably distorted.

In comparison to the projection and VPM techniques discussed earlier, the time-dependent approach is substantially faster numerically; moreover, any potential $U(x_1, x_2)$ can be considered with ease in this approach. One has to keep in mind, however, that it is not always easy to provide quantitative answers to stationary state questions such as the determination of scattering phase shifts in this example, using the time-dependent techniques. The exact choice of the initial state as well as

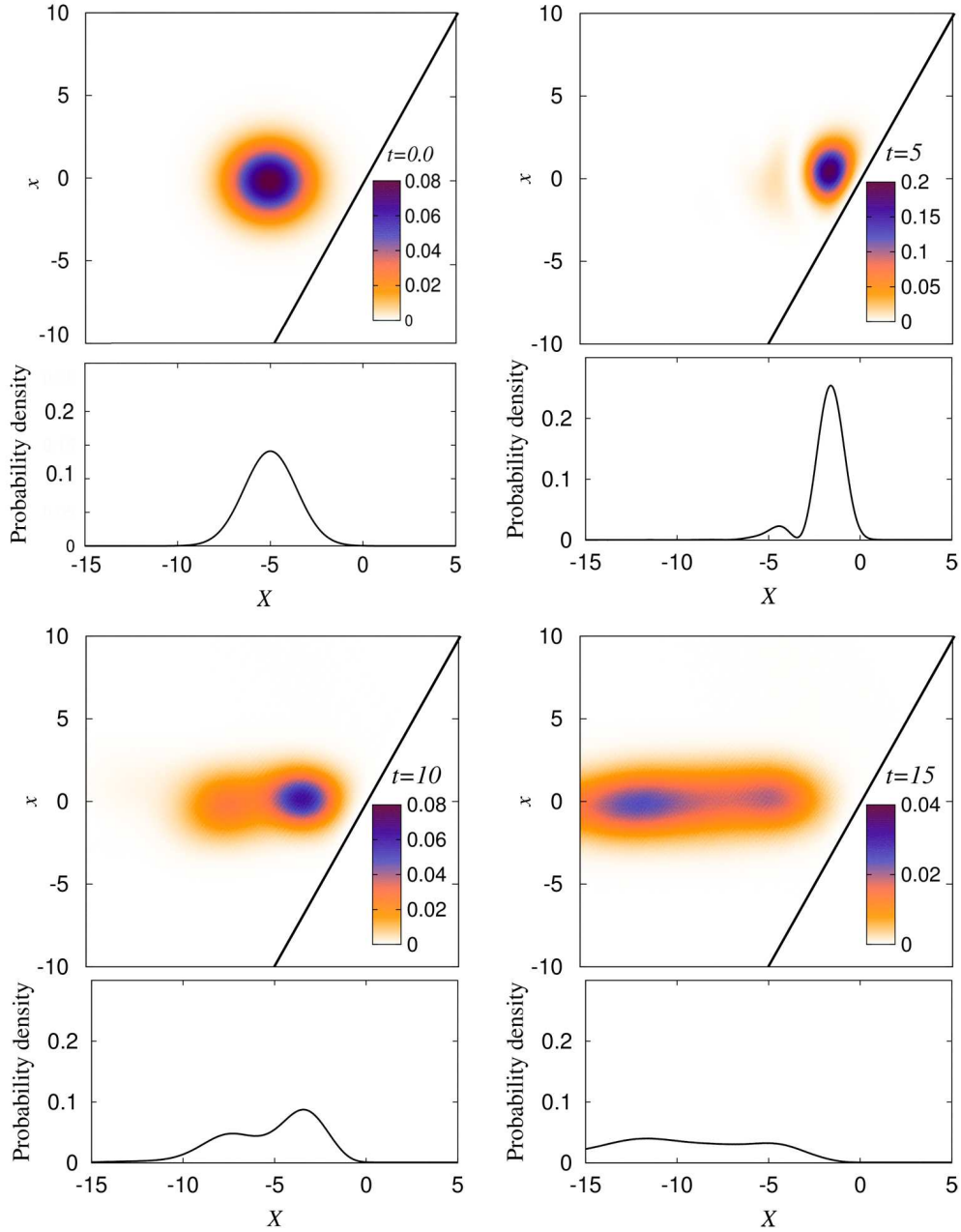


Figure 5: The four panels show the wave function $|\Phi(X, x)|^2$ as a density plot for different times $t = 0, 5, 10$ and 15 , as labeled. For each of the time snapshots, the lower plot shows the density distribution over the center-of-mass coordinate computed as $\int |\Phi(X, x)|^2 dx$. The initial wave function at $t = 0$ is given by the Gaussian wave packet, Eq. (15). For this system $\mu_1 = \mu_2$, the border of inaccessible area $x_2 > 0$ is shown with a solid line.

the energy uncertainty of the initial state can be important for some stages of time evolution.

The physics of decay of unstable states represents a particularly important class of time-dependent processes. The familiar exponential decay law is only an incomplete picture requiring some subtle approximations, and being valid only within certain time limits. The complex intrinsic dynamics that can occur in the decaying many-body system, further complicates the time evolution. Non-exponential decay laws in

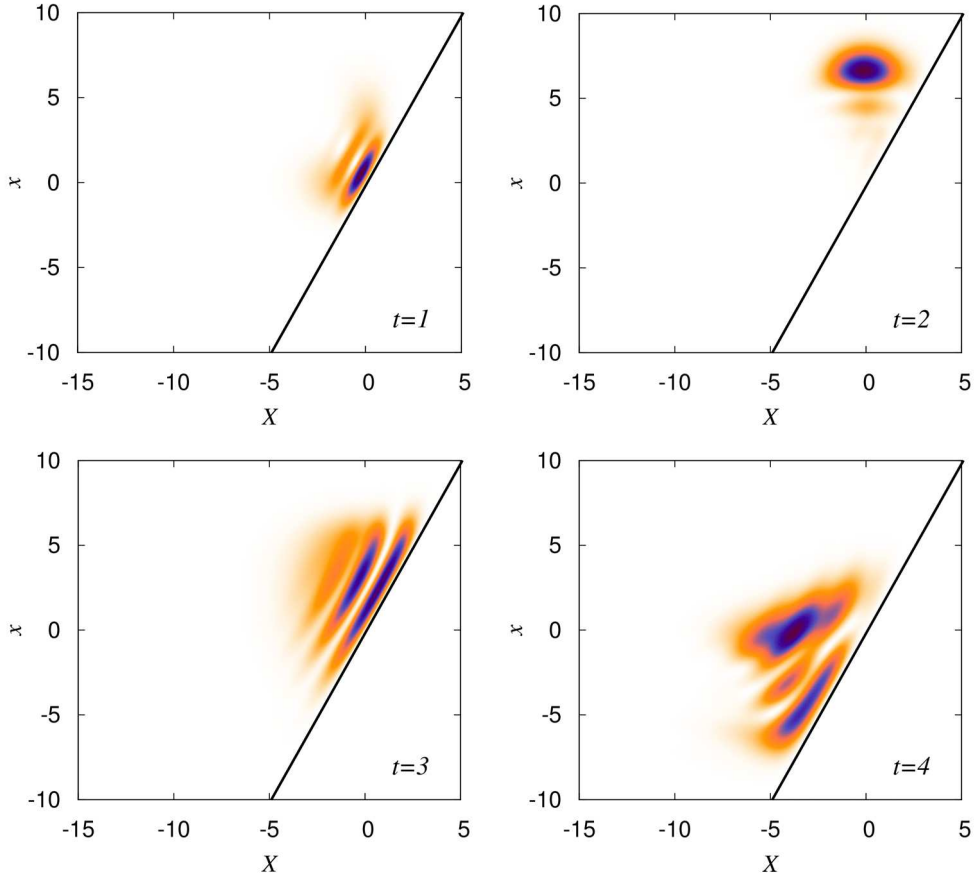


Figure 6: The four panes similar to those in Fig. 5, show the wave function $|\Phi(X, x)|^2$ at the most representative moments of time $t = 1, 2, 3$ and 4 , during the high energy collision with the impenetrable wall. Here $K_0 = 5$, the remaining parameters being the same as in Fig. 5.

quantum mechanics have been studied and revisited by many authors (see Ref. [3] and references therein). The presence of three regimes, namely, the initial, the exponential, and the long-time power law, appears to be a universal feature of decay processes. The transitions from one regime to another are accompanied by the interference of corresponding quantum amplitudes that is seen as oscillations on the decay curve.

As another demonstration of the time-dependent technique based on the Trotter–Suzuki expansion and as an introduction to the section that follows, we demonstrate in Fig. 7 the decay process in Winter’s model [11] which has been a very popular tool for exploring non-exponential features in decays. In this model, a particle is confined to the region $x \geq 0$ by the impenetrable wall at $x = 0$ and is held by a delta barrier at $x = 1$. The initial state at $t = 0$ is taken as $\Psi(x, 0) = \sqrt{2} \sin(\pi x)$. The survival probability shown by a solid red line in the left panel of Fig. 7, illustrates three general regimes: the pre-exponential, the exponential, and the post-exponential. Oscillations can be seen in transitional regions. The snapshots of the wave function at different times are shown on the right.

The pre-exponential behavior at very early times is influenced by the memory of how the state was created and, in particular, by the high energy components of the state. Later in time, the internal structure and transitions between the intrinsic states become relevant. Short times correspond to remote energy components where the presence of other resonant states is to be considered. The high energy components have much shorter lifetimes and decay quickly leading to the exponential decay phase.

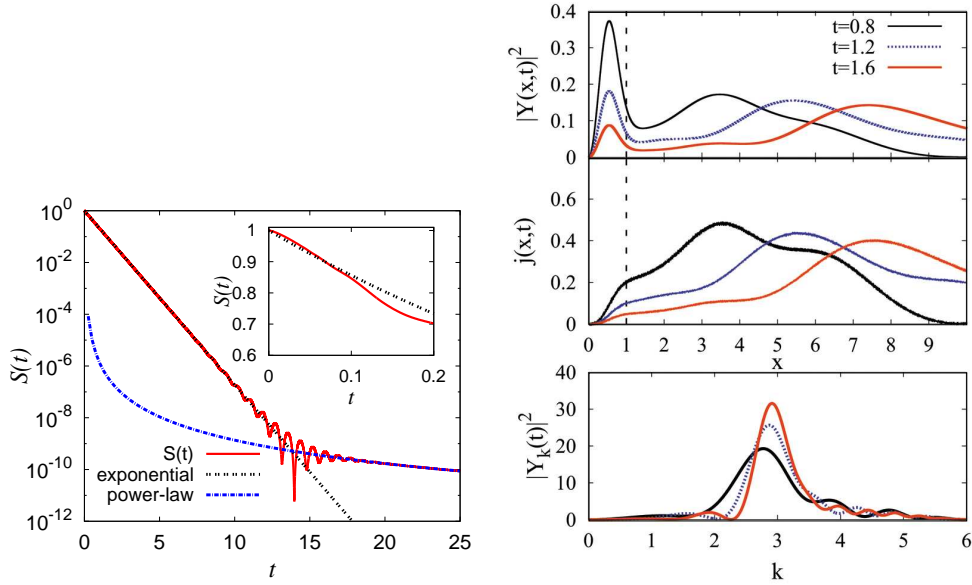


Figure 7: Left: the survival probability $S(t) = |\langle \Psi(0) | \Psi(t) \rangle|^2$ is shown as a function of time (solid red line). The exponential decay law where the mean lifetime $\tau = 0.65$ is known from the poles of the scattering matrix, is shown with a double-dotted black line, the background component that decays following a power law is shown with a dot-dash blue line. The survival probability at very early times is shown in the inset. Right: the wave function of a decaying state is shown at times $t = 0.8, 1.2,$ and 1.6 : the upper panel shows the probability distribution $|\Psi(x,t)|^2$, the middle panel displays the current $j(x,t)$, and the wave function in momentum space is shown in the lower panel. Here the strength of the delta function $G = 6$ in units where $\hbar = 2m = 1$.

This phase is dominated by a single resonant component, the radiating state, so that the wave function retains its shape while decreasing in amplitude. This can be seen in the right panel of Fig. 7. In the same figure, one can also trace a moving away background component. The background contains very low energy particles; being far off-resonance, they essentially do not interact but move slowly away from the interaction region. Near the decay threshold, the number of such particles with a certain energy is determined by the available phase space, which for neutral particles scales with energy following a power-law $E^{l+1/2}$ where l is the angular momentum quantum number. This type of scaling leads to non-resonant components that follow a power-law decay $S(t) \sim 1/t^{2\ell+3}$. While the non-resonant component can be very small in the initial state, eventually it becomes dominant due to its slower-than-exponential decay. Further discussion of decay processes in quantum mechanics and other examples can be found in Ref. [3]. The near-threshold phase space scaling with energy which leads to power-law decay at remote times, is an important consideration in the Time-Dependent Continuum Shell Model approach that is discussed in the following section, see also Refs. [1, 12, 13], as well as in more complicated sequential decay processes [14].

3 Time-Dependent Continuum Shell Model

3.1 Continuum Shell Model

A seamless transition between structure physics and reactions is one of the central present-day theoretical problems. The computational aspect associated with transitions from discrete levels to a continuum of reaction states is especially challeng-

ing. The Continuum Shell Model approach [12, 13] and its time-dependent version in particular, is one among several theoretical tools confronting these issues. In the Continuum Shell Model, the Feshbach projection formalism [15, 16] is used to express the exact dynamics in the full Hilbert space using an effective Hamiltonian in the projected intrinsic subspace of interest, \mathcal{Q} :

$$\mathcal{H}(E) = H_{\mathcal{Q}\mathcal{Q}} + \tilde{H}(E), \quad (16a)$$

where

$$\tilde{H}(E) = H_{\mathcal{Q}\mathcal{P}} \frac{1}{E - H_{\mathcal{P}\mathcal{P}}} H_{\mathcal{P}\mathcal{Q}}. \quad (16b)$$

Here the effective Hamiltonian contains $H_{\mathcal{Q}\mathcal{Q}}$ which is the part of the original Hamiltonian that acts in the space \mathcal{Q} , and the energy-dependent non-Hermitian term $\tilde{H}(E)$ that emerges from the coupling of the space \mathcal{Q} to the external space containing the continuum of reaction states, \mathcal{P} .

In practical applications the intrinsic space \mathcal{Q} is assumed to represent the configuration space of the traditional shell model built from states $|1\rangle$ that are Slater determinants constructed from bound-state single-particle wave functions. The space \mathcal{P} contains continua of reaction states $|c, E\rangle$ characterized by the channel index, c , and the continuous energy parameter, E . There is a certain threshold energy $E_{\text{thr}}^{(c)}$ for each channel c . The energy-dependent non-Hermitian effective Hamiltonian (16) is represented by a matrix $\mathcal{H}_{12}(E) \equiv \langle 1|\mathcal{H}(E)|2\rangle$,

$$\mathcal{H}_{12}(E) = H_{12} + \Delta_{12}(E) - \frac{i}{2}W_{12}(E), \quad (17a)$$

where

$$\Delta_{12}(E) = \sum_c \text{PV} \int_{E_{\text{thr}}^{(c)}}^{\infty} dE' \frac{A_1^c(E')A_2^{c*}(E')}{E - E'}, \quad (17b)$$

$$W_{12}(E) = 2\pi \sum_{c(\text{open})} A_1^c(E)A_2^{c*}(E), \quad (17c)$$

and the channel amplitudes are the matrix elements $A_1^c(E) = \langle 1|H|c, E\rangle$. The traditional shell model Hamiltonian is recovered when the internal space \mathcal{Q} is isolated and thus decoupled, $A_1^c(E) = 0$.

Computational challenges of the traditional shell model approach are well known, they are mainly associated with the need to find some selected eigenvalues and eigenvectors of the Hamiltonian matrix H_{12} . The matrix is generally sparse, thanks to few-body nature of the underlying nucleon-nucleon interactions which inhibit mixing of very remote configurations, thus iterative techniques such as Lanczos approach are commonly used.

The physics of weakly-bound and unstable nuclear systems is much more rich as questions of interest span from properties of bound states to features in scattering cross sections. Narrow resonances are well characterized by usual properties of bound states with the decay width being an additional characteristic. This requires the non-Hermitian eigenvalue problem $\mathcal{H}(E)|\mathcal{I}\rangle = \mathcal{E}|\mathcal{I}\rangle$ to be solved. The resulting complex energies \mathcal{E} represent positions of resonances, $E = \text{Re}(\mathcal{E})$, and their widths, $\Gamma = -2\text{Im}(\mathcal{E})$. The most practical technique here is to start with a perturbative treatment and evaluate the term $\tilde{H}(E)$ associated with continuum using wave functions of the traditional shell model Hamiltonian $H_{\mathcal{Q}\mathcal{Q}}$. As coupling to the continuum increases the states become broad and one is forced to treat the non-Hermitian energy-dependent eigenvalue problem as an iterative non-Hermitian diagonalization process. In this limit, a major problem is associated with the physical interpretation of the resonances and their widths.

Formally, the energy-dependent non-Hermitian Hamiltonian provides an exact propagator for the intrinsic space, and therefore the scattering matrix is

$$\mathbf{S}_{cc'}(E) = \exp(i\xi_c + i\xi_{c'}) [\delta_{cc'} - 2\pi i \mathbf{T}_{cc'}(E)], \quad (18a)$$

where

$$\mathbf{T}_{cc'}(E) = \sum_{12} A_1^c(E) \left\{ \frac{1}{E - \mathcal{H}} \right\}_{12} A_2^{c'}(E). \quad (18b)$$

Here ξ_c is a potential (direct-reaction) phase. The matrix is unitary (see Ref. [1]) and the unitarity is related to the factorized form of the imaginary $W_{12}(E)$ in Eq. (17). The eigenvalues of the non-Hermitian Hamiltonian are therefore the poles of the scattering matrix. In the limit of broad resonances, one has to address the reaction problem where obtaining a reaction cross section is the main goal. There are several numerical challenges associated with Eq. (18), many of these challenges being similar to the ones discussed in Section 2.1. First, the size of the Hamiltonian matrix and the complex arithmetic involved are not making this problem simpler as compared to matrix diagonalization. Second, the scattering energy E represents a running parameter so that the procedure should be repeated for all energies of interest. Finally, the problem is numerically unstable: bound states as well as resonances with widths ranging by many orders of magnitude, may be encountered and should be treated consistently. All of these technical issues are resolved by the Time-Dependent Continuum Shell Model approach which we discuss next.

3.2 Time-dependent many-body evolution operator

The many-body wave function follows the time evolution which is a Fourier image of the retarded propagator involved in the scattering matrix (18):

$$G(E) = \frac{1}{E - H} = -i \int_0^\infty dt \exp(iEt) \exp(-iHt). \quad (19)$$

Here H is an arbitrary Hamiltonian but, as discussed below, it is advantageous to include a factorized imaginary part W using a different procedure described in Section 3.3. Thus we view H as being a Hermitian Hamiltonian of the traditional shell model in which case it is set to have an infinitesimal negative-definite imaginary part. The time-dependent evolution operator can be factorized using a Chebyshev polynomial expansion method, see Ref. [1, 17, 18]:

$$\exp(-iHt) = \sum_{n=0}^{\infty} (-i)^n (2 - \delta_{n0}) J_n(t) T_n(H), \quad (20)$$

where J_n is the Bessel function of the first kind and T_n represents Chebyshev polynomials. The Chebyshev polynomials defined as $T_n[\cos(\theta)] = \cos(n\theta)$ or, in explicit form,

$$T_n(x) = \frac{n}{2} \sum_{k=0,1,\dots}^{k \leq n/2} \frac{(-1)^k}{n-k} \binom{n-k}{k} (2x)^{n-2k}, \quad (21)$$

provide a complete set of orthogonal functions covering uniformly the interval $[-1, 1]$. In contrast, Taylor expansion relies on power functions which favor the edges of the interval and thus are more sensitive to extreme eigenvalues. The ‘‘angular addition’’ identity

$$2T_n(x)T_m(x) = T_{n+m}(x) + T_{n-m}(x), \quad n \geq m, \quad (22)$$

which follows from the definition, allows one to obtain these polynomials using the recurrence relation

$$T_0(x) = 1, \quad (23a)$$

$$T_1(x) = x, \quad (23b)$$

$$T_{n+1}(x) = 2xT_n(x) - T_{n-1}(x). \quad (23c)$$

Therefore the process of evaluation of Chebyshev polynomials of the Hamiltonian operator is an iterative procedure similar to that in Lanczos approach. For a given initial state $|\lambda\rangle \equiv |\lambda_0\rangle$, a sequence $|\lambda_n\rangle = T_n(H)|\lambda\rangle$ can be constructed as

$$|\lambda_0\rangle = |\lambda\rangle, \quad (24a)$$

$$|\lambda_1\rangle = H|\lambda\rangle, \quad (24b)$$

and

$$|\lambda_{n+1}\rangle = 2H|\lambda_n\rangle - |\lambda_{n-1}\rangle. \quad (24c)$$

For overlap functions, assuming Hermitian H , one can also use the following identity:

$$\langle\lambda'|T_{n+m}(H)|\lambda\rangle = 2\langle\lambda'_m|\lambda_n\rangle - \langle\lambda'|\lambda_{n-m}\rangle, \quad n \geq m. \quad (25)$$

A well-controlled energy resolution is an advantage of the method. In applications of the method, the energy interval $[E_{min}, E_{max}]$ which should contain all eigenvalues of H , is mapped onto $[-1, 1]$ by rescaling the Hamiltonian as $H \rightarrow (H - \bar{E})/\Delta E$, where $\bar{E} = (E_{max} + E_{min})/2$ and $\Delta E = (E_{max} - E_{min})/2$. For a desired energy resolution $\Delta E/N$ where N is some even integer number, the discrete Fourier transform allows one to evaluate Green's function in the corresponding energy points of the rescaled interval $E_p = p/N$ with $p = -N/2, \dots, N/2$,

$$\langle\lambda'|G(E_p)|\lambda\rangle = -i\pi \left\{ \sum_{\tau=0}^{N-1} e^{2\pi ip\tau/N} \sum_{n=0}^{n_{\max}(\tau)} (-i)^n (2 - \delta_{n0}) J_n(\pi\tau) \langle\lambda'|T_n(H)|\lambda\rangle \right\}. \quad (26)$$

This requires the evaluation of the evolution operator at times $t = \pi\tau$, where $\tau = 0, \dots, N-1$. For each desired time point τ the number of terms in expansion (20) needed for the convergence, is denoted as $n_{\max}(\tau)$. The Bessel function asymptotics $J_n(x) \approx \sqrt{1/(2\pi n)} [ex/(2n)]^n$ suggests $n_{\max}(\tau) \approx e\pi\tau/2 \approx 4\tau$. At fixed values of n but for large times the convergence remains stable due to $J_n(t) \approx \sqrt{2/(\pi t)} \cos(t - \pi n/2 - \pi/4)$ in this limit. For the desired energy resolution $\Delta E/N$, the propagation in time has to be extended up to $\approx \tau N$ which requires $n_{\max} \approx 4N$; therefore $2N$ matrix-vector multiplications are required if one also uses Eq. (25).

The time-dependent approach provides the Green's function for all energies at once; it is also exceptionally stable numerically when dealing with very narrow resonances or with stable states. Indeed, the time-dependent behavior of stationary states is regular and the corresponding delta function in energy is well handled by Fourier transform which at the desired energy resolution properly conserves the integrated strength.

In order to illustrate the approach, let us consider strength and integrated strength functions defined for a given state $|\lambda\rangle$ as

$$F_\lambda(E) = \langle\lambda|\delta(E - H)|\lambda\rangle = -\frac{1}{\pi} \text{Im} \langle\lambda|G(E)|\lambda\rangle, \quad (27a)$$

$$I_\lambda(E) = \int_{-\infty}^E F_\lambda(E') dE'. \quad (27b)$$

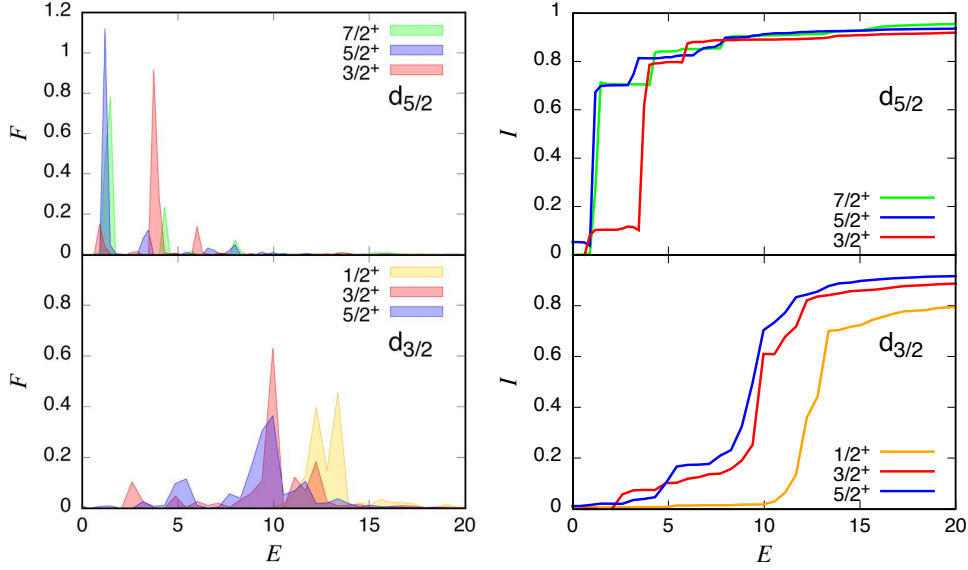


Figure 8: Single-particle strength function (left) and cumulative or integrated strength function (right) are shown as functions of excitation energy (in units of MeV) for ^{15}N .

In Fig. 8 both the strength (left) and the integrated strength (right) functions are shown for ^{15}N for neutron channels where $|\lambda\rangle$ corresponds to different angular momentum channels constructed from the 1^+ ground state in ^{14}N coupled to a single nucleon on either $d_{5/2}$ (top panels) or $d_{3/2}$ (bottom panels) single-particle states. This theoretical study follows recent experimental work in Ref. [19]. The full p - sd valence space is used with the Hamiltonian from Ref. [20]. With about 10^7 m -scheme basis states, obtaining and computing strength functions in energy regions around 20 MeV of excitation is impractical; the time-dependent method provides an excellent alternative.

3.3 Sherman–Morrison–Woodbury relations

It is certainly possible to implement the Chebyshev polynomial expansion procedure for the full non-Hermitian Hamiltonian using Eq. (20); however the factorized structure of \tilde{H} offers a different alternative which is much more computationally advantageous. The two propagators corresponding to Eqs. (16),

$$G(E) = \frac{1}{E - H_{QQ}} \quad (28a)$$

and

$$\mathcal{G}(E) = \frac{1}{E - \mathcal{H}(E)}, \quad (28b)$$

can be related through the Dyson equation $\mathcal{G}(E) = G(E) + G(E)\tilde{H}(E)\mathcal{G}(E)$. Since the contribution from the continuum emerges in the factorized form

$$\tilde{H}(E) = \sum_{cc'} |c\rangle \tilde{\mathbf{H}}_{cc'}(E) \langle c'|, \quad (29)$$

the expression for the full propagator can be found in a closed form in the space spanned by the channel states:

$$\mathbb{G} = \mathbf{G} \left[\mathbf{1} - \tilde{\mathbf{H}}\mathbf{G} \right]^{-1} = \left[\mathbf{1} - \mathbf{G}\tilde{\mathbf{H}} \right]^{-1} \mathbf{G}. \quad (30)$$

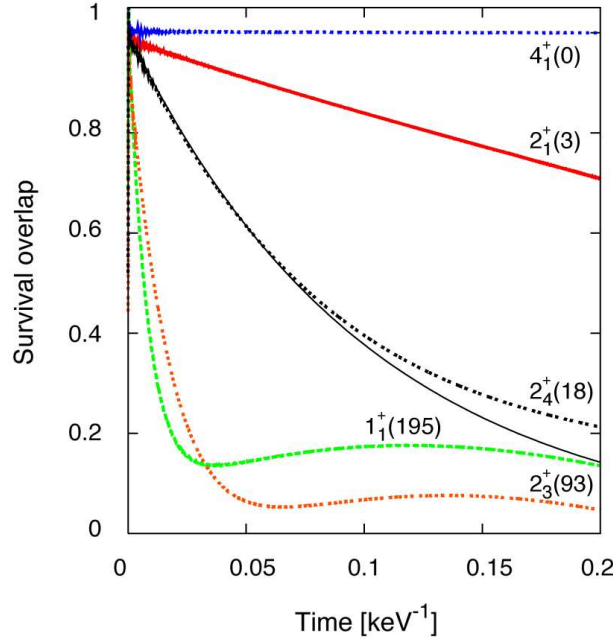


Figure 9: Time evolution of several low-lying states in ^{24}O . The absolute value of the survival overlap $|\langle\alpha|\exp(-i\mathcal{H}t)|\alpha\rangle|$ is shown as a function of time. Different lines, as marked, correspond to states $\alpha(E_\alpha, \Gamma_\alpha)$: 2_1^+ (4.180, 2.7), 1_1^+ (5291, 195.1), 4_1^+ (6947, 0.0), 2_3^+ (8107, 92.5) and 2_4^+ (9673, 17.5). They are eigenstates of the traditional USD shell model but are non-stationary resonances in the Time-Dependent Continuum Shell Model, except for the 4_1^+ state which due to its high spin does not decay within the sd valence space. To emphasize the non-exponentiality in the decay law, the unmarked solid line shows the $\exp(-\Gamma_\alpha t/2)$ function with parameters for the 2_4^+ state.

The operators here are represented by matrices in the channel subspace $\mathbb{G}_{ab} = \langle a|\mathcal{G}(E)|b\rangle$ and $\mathbf{G}_{ab} = \langle a|G(E)|b\rangle$. In computer science these relations are known as Sherman–Morrison–Woodbury matrix inversion equations [21]. The unitarity of the scattering matrix immediately follows from these relations, see [1].

We illustrate the Time-Dependent Continuum Shell Model approach in its complete form in Figs. 9 and 10 where the resonances in ^{24}O are considered. The system is treated in the sd valence space using the USD shell model Hamiltonian [22]. In Fig. 9 the norm of the survival amplitude is shown as a function of time for the following set of most representative states: 2_1^+ (4180, 2.7), 1_1^+ (5291, 195.1), 4_1^+ (6947, 0.0), 2_3^+ (8107, 92.5), and 2_4^+ (9673, 17.5). The states are listed here with their excitation energies followed by the decay widths, both in keV. The initial wave functions at $t = 0$ are taken as eigenstates of the traditional shell model. For the states such as 4_1^+ which cannot decay in this model due to high angular momentum, the norm of the survival amplitude remains constant. Narrow states exhibit a nearly exponential decay, for the state 2_4^+ the survival amplitude expected in exponential decay is shown. The decay is non-exponential for broad states such as 1_1^+ and 2_3^+ . In Fig. 10 the scattering cross section is shown for elastic neutron scattering on the ground state of ^{23}O where the same resonant states can be observed.

The time-dependent approach provides an effective computational strategy for treating many-body systems that feature both bound and unbound states. In contrast to the stationary state formalism, the time dependent approach addresses the evolution of states in a natural way, thus providing a computationally robust and stable strategy where experimental observables are easily recovered and fundamental

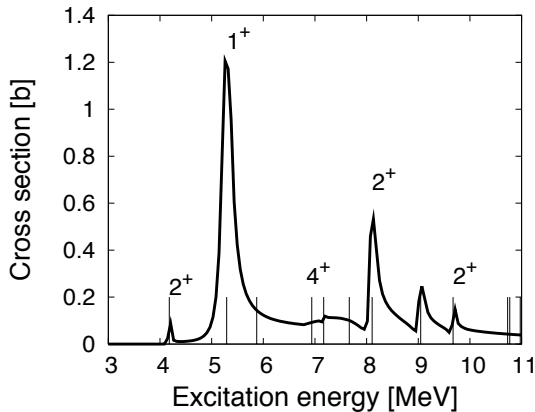


Figure 10: Scattering cross section for $^{23}\text{O}(n, n)^{23}\text{O}$ reaction showing resonances in ^{24}O .

principles of quantum mechanics, such as linearity and unitarity, are followed. From the computational perspective, the most efficient operation available for the matrix-vector multiplication is utilized in building the time evolution operator with full control of the desired energy and time resolution. The specifics of the terms that emerge due to coupling to continuum in Feshbach projection formalism can be used to build the full evolution operator using Sherman–Morrison–Woodbury relations. The Time-Dependent Continuum Shell Model found broad practical applications, see Refs. [23–25] for examples.

4 Conclusions

As our interests shift towards open, reacting, decaying, and otherwise evolving quantum many-body systems, new theoretical and computational techniques must be developed to address multiple new challenges that emerge. The goal of this presentation is to highlight some of the methods used in the recent scientific projects. We use a simple model to demonstrate three distinctly different techniques. The most straightforward method involves projecting the dynamics onto a set of basis states, allowing subsequently for the well-developed methods of linear algebra to be used; in certain reaction problems this method appears to have significant drawbacks associated with numerical instabilities and poor convergence. We demonstrate the Variable Phase Method that can treat reaction problems efficiently in a discretized coordinate space. Finally, we consider explicitly time-dependent techniques that are perhaps most adequate for the time-dependent dynamics associated with decay. We put forward the Time-Dependent Continuum Shell Model approach as a practical tool and demonstrate its application to realistic problems in nuclear physics.

This material is based upon work supported by the U.S. Department of Energy Office of Science, Office of Nuclear Physics under Award Number DE-SC0009883. The author is grateful to N. Ahsan, M. Peshkin, and V. Zelevinsky for collaboration.

References

- [1] A. Volya, Phys. Rev. C **79**, 044308 (2009).
- [2] N. Ahsan and A. Volya, Phys. Rev. C **82**, 064607 (2010).
- [3] M. Peshkin, A. Volya and V. Zelevinsky, EPL **107**, 40001 (2014).
- [4] N. Ahsan and A. Volya, J. Phys. Conf. Ser. **312**, 092011 (2011).
- [5] A. Sakharuk and V. Zelevinsky, A toy model for the scattering of composite objects, in *APS Ohio Section Fall Meeting, 1999APS..OSF..CD09S* (1999).

-
- [6] A. M. Moro, J. A. Caballero and Gómez-Camacho, arXiv:1010.4933 [nucl-th] (2010).
- [7] V. V. Babikov, *Method of phase functions in quantum mechanics*. Nauka, Moscow, 1968 (*in Russian*).
- [8] W. van Dijk, J. Brown and K. Spyksma, Phys. Rev. E **84**, 056703 (2011).
- [9] H. F. Trotter, Proc. Am. Math. Soc. **10**, 545 (1959).
- [10] M. Suzuki, Phys. Lett. A **146**, 319 (1990).
- [11] R. G. Winter, Phys. Rev. **123**, 1503 (1961).
- [12] A. Volya and V. Zelevinsky, Phys. Rev. Lett. **94**, 052501 (2005).
- [13] A. Volya and V. Zelevinsky, Phys. Rev. C **74**, 064314 (2006).
- [14] A. Volya, EPJ Web Conf. **38**, 03003 (2012).
- [15] H. Feshbach, Ann. Phys. (NY) **5**, 357 (1958).
- [16] C. Mahaux and H. A. Weidenmüller, *Shell-model approach to nuclear reactions*. North-Holland, Amsterdam, London, 1969.
- [17] Y. L. Loh, S. N. Taraskin and S. R. Elliott, Phys. Rev. E **63**, 056706 (2001).
- [18] T. Ikegami and S. Iwata, J. Comp. Chem. **23**, 310 (2002).
- [19] C. E. Mertin *et al.*, Acta Phys. Pol. B **45**, 159 (2014).
- [20] Y. Utsuno and S. Chiba, Phys. Rev. C **83**, 021301(R) (2011).
- [21] W. H. Press, S. A. Teukolsky, W. T. Vetterling and B. P. Flannery, *Numerical recipes in C++: the art of scientific computing*. Cambridge University Press, Cambridge, New York, 2002.
- [22] B. A. Brown, W. A. Richter, R. E. Julies and B. H. Wildenthal, Ann. Phys. (NY) **182**, 191 (1988).
- [23] J. P. Mitchell *et al.*, Phys. Rev. C **87**, 054617 (2013).
- [24] J. P. Mitchell *et al.*, Phys. Rev. C **82**, 011601(R) (2010).
- [25] G. V. Rogachev *et al.*, Phys. Rev. C **75**, 014603 (2007).